JOURNAL OF EXPERIMENTAL AND THEORETICAL PHYSICS, 2024, Vol. 165, No. 2, pp. 189–197

ATOMS, MOLECULES, OPTICS

STABILIZATION OF FEMTOSECOND PULSE GENERATION IN A LASER WITH PASSIVE MODE SYNCHRONIZATION ON A $Mg_2SiO_4 : Cr^{4+}$ CRYSTAL DUE TO SPECTRAL UNLOADING OF THE RESONATOR INTO KELLY SIDE COMPONENTS

© 2024 A.A. Ivanov[a,b,c], A. A. Lanin[b,c], A. A.Voronin[b,c] E. V. Zharikov[d], A. B. Fedotov[b*]

[a] *Photochemistry center, FSRC "Crystallography and Photonics" RAS, Moscow 119333, Russia*
[b] *Lomonosov Moscow State University, Moscow 119992, Russia*
[c] *Russian Quantum Center, Skolkovo 143025, Moscow Region, Russia*
[d] *Prokhorov General Physics Institute of RAS, Moscow 119991, Russia*

**e-mail: a.b.fedotov@physics.msu.ru*

Received September 26, 2023
Revised October 16, 2023
Accepted October 18, 2023

Abstract. Increasing the efficiency and stability of femtosecond pulses generation in solid-state lasers has great significance for technological processes. At the same time, there is a need for research into a number of physical issues. The variable action of the instantaneous Kerr nonlinearity in the crystal, necessary for passive mode locking of the resonator, and the dispersion of the prisms, providing generation of ultrashort pulses, inevitably leads to regular perturbation of the shape of the generated pulses. In our work, we study the loss transformation regimes in a passive mode locking femtosecond laser pulses oscillator on a $Mg_2SiO_4:Cr^{4+}$ crystal (chromium-forsterite) when the intracavity peak field power of the order of 2 MW, close to the critical self-focusing power. Analysis of the spectra and pulse durations in various parts of the cavity shows that the quasi-soliton pulse generation regime with the maximum peak power for the laser is supported by removing excess energy from the cavity through the generation of spectral Kelly sidebands and broadening the pulse spectrum beyond the gain of the active medium. A strong broadening of the pulse spectrum in the crystal upsets the balance of dispersive and nonlinear phase shifts and leads to deformation of the generated pulse shape. Additional passive losses arising due to nonlinear transformation in the crystal significantly reduce the efficiency of laser generation and limit peak power of the pulses.

Keywords: *femtosecond chromium-forsterite laser, Kelly sidebands*

DOI: 10.31857/S00444510240205e2

1. INTRODUCTION

Ultra-short laser pulses have been widely used for two decades in fundamental physical research: in the field of interaction of extreme electric fields with matter [1, 2], material sciences [3], astronomy [4], and metrology [5]. The development of femtosecond pulse sources has led to new methods of noninvasive visualization of biological tissues with subcellular spatial resolution based on classical phenomena of nonlinear optics: generation of optical harmonics and two-photon excitation of fluorescence [6, 7]. Combining several techniques into a multimodal imaging tool opens up a wide range of possibilities for optical biopsy [8], intraoperative histology [9], and lifetime markerless imaging [10, 11], but places high demands on the parameters of the laser source. Femtosecond pulse generators on $Mg_2SiO_4:Cr^{4+}$ (chrome forsterite) crystal [12] occupy a special place in multiphoton microscopy and nonlinear spectroscopy of living systems due to the fact that radiation at a central wavelength of 1.25 μm has a relatively large penetration depth into biological tissues, which makes it possible to reconstruct the spatial distribution of fluorescent markers from a great depth under two-photon excitation, and the generated second and third harmonics fall into the tissue transparency regions near 630 nm and 420 nm [13, 14, 15, 16]. Increasing

the peak power of oscillator pulses is particularly important for increasing the sensitivity of nonlinear optical spectroscopy and radically increasing the depth of microscopy imaging due to three-photon excitation of fluorescence [17, 18, 19, 20].

High peak power of the laser output pulses is achieved with increasing energy and decreasing pulse duration at careful tuning of the total dispersion of the resonator group delays (GDD), equal to the sum of the dispersion of the second-order group delays of each resonator element, over the entire wavelength range of the crystal gain bandwidth. In a typical soliton-like laser with passive mode synchronization, the added energy that the pulse receives at each resonator bypass in the active medium does not fully correspond to the temporal and spectral profile of the fundamental soliton. Periodic perturbations of dispersion, nonlinearity, and amplification of the pulse during its propagation in the laser resonator lead to the fact that, due to phase matching and different group velocities of the soliton pulse and dispersion waves [21] (DW, low-intensity light waves), part of the soliton energy inevitably flows into dispersion waves in the process of the amplified pulse acquiring the necessary shape to realize the balance of the effect of nonlinearity and dispersion on the pulse. This is most clearly manifested in fiber pulse lasers as the formation of symmetric Kelly spectral components due to the physical processes of nonlinear phase modification and relatively weak amplification stretched along the bulk of the resonator [22, 23, 24]. The exponential growth of such parasitic components at the edges of the soliton spectrum leads to competition for pump energy and nonlinear cross-interaction with the main pulse, manifested in power instability and loss of generation of soliton-like pulses [25]. The limited effect of the Kelly spectral components in fiber lasers on generation is explained by the relatively small gain width of light guides doped with rare-earth metal ions [26]. However, the introduction of additional losses at Kelly component wavelengths using spectral filters can improve laser stability: reduce power noise, time jitter, and increase the time contrast of the intensity envelope [27, 28]. In solid-state lasers, Kelly components can also have a negative effect on the stability of pulsed laser generation, although it is more difficult to observe them due to the spaced nonlinear effects on the pulse and its compensation in the prism compressor or chirped mirrors. In femtosecond lasers on chrome forsterite crystals, nonlinear phase raid is more pronounced than in other solid-state lasers because of the use of longer active elements due to the relatively low pump absorption coefficient [29, 30]. This inevitably leads to spectrum broadening, nonlinear optical conversion of the pulse, and additional passive losses. Selective removal of radiation from the resonator at the frequencies of the generated Kelly components can increase the energy of the supported quasi-soliton pulse.

In this work, we study the effect of unloading the resonator of a laser on a chromium-forsterite crystal with passive mode synchronization on the Kerr nonlinearity, generating quasi-soliton pulses with duration up to 30 fs and intracavity peak power up to 2.2 MW, accompanied by strong Kelly components, on the ability to maintain a stable mode of generation under strong pumping. The spectra and durations of radiation at different points of the resonator at varying the transmission coefficient of the output mirror have been investigated. The influence of phase self-modulation of pulses on the limiting intensity of generated pulses was shown. It is shown that at generation of extremely short pulses of high intensity in the chromium-forsterite crystal there is a spectral transformation of pulses leading to the growth of passive losses in the laser resonator.

2. MATERIALS AND METHODS

Experimental studies of the peculiarities of the formation of Kelly spectral components in a solid-state laser were carried out on a mockup of a femtosecond chromium-forsterite laser with passive mode synchronization on the Kerr nonlinearity, assembled according to a standard Z-shaped scheme to compensate for beam aberrations in the active element with the possibility to vary the output mirrors M1 (Fig. 2 *a*). The pump radiation of a 14 W ytterbium fiber laser (IRE-Polus, Russia) was focused by a lens with a focal length of 15 cm through a spherical mirror M2 into a 15 mm long Mg_2SiO_4:Cr^{4+} crystal maintained at +5°C with the ends cut at a Brewster angle. The absorption coefficient of the crystal at a wavelength of 1064 nm was 1 cm^{-1}. Collimation of luminescence from the crystal was accomplished by spherical mirrors M2 and M3 with a radius of curvature of 15 cm. A pair of nearly equilateral prisms made of SF14 glass, spaced 35 cm apart, was used to compensate for the normal dispersion of the group delays of the resonator and to fine-tune the dispersion. The flat mirror M5, outputting the long-wavelength radiation from the resonator, had a transparency boundary at a wavelength of 1490 nm.

The radiation characterization was carried out behind the output mirror M1 and mirror M5. The spectra were recorded by an InGaAs spectrometer

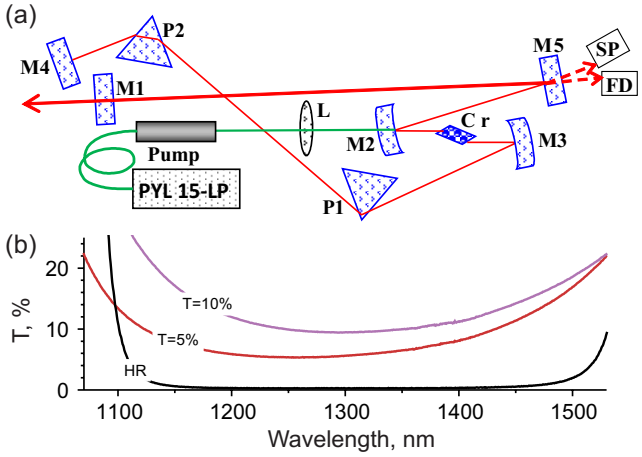

Fig 1. *a* – Optical scheme of the laser resonator: M1 – output mirror, M2, M3 – spherical mirrors with radius of curvature 15cm; M4, M5 – flat mirrors; P1, P2 – prisms made of SF14 glass; Cr – crystal $Mg_2SiO_4:Cr^{4+}$; Pump – collimator of ytterbium fiber pump laser PYL15-LP; L – pump radiation lens with focal length 15cm; SP – spectrometer; FD – FD-2G avalanche-mode LED. *b* – Spectral characteristics of 10%, 5%, and 0.2% output mirrors.

SDH-IV (SOLAR LS, Republic of Belarus). The correlation functions of pulses were recorded with a scanning autocorrelator AA-M (Avesta-Project, Russia). The average radiation power was registered by a 407-A thermal power meter (Spectra-Physics, USA). The pulse repetition rate was 100 MHz and was controlled by an avalanche-mode germanium photodiode FD-2G (USSR). In this work, we analyzed the pulse generation features and Kelly spectral components during passive mode synchronization in the laser at a fixed pump level and varying the transmittance of the M1 output mirror from 10% to 0.2% in the 1200-1350 nm window (Fig. 1 *b*). For each output mirror, the laser resonator was tuned to the maximum average power in the stable pulse generation mode. The output average laser power in the femtosecond generation mode was approximately 5-10% higher than in the continuous generation mode for the same alignment of the optical elements of the resonator. Discrimination of such a level between continuous and pulsed modes ensured stable operation of the laser in the pulsed mode. The laser switched from continuous to pulse mode spontaneously or at a slight fluctuation caused by a light impact on the optical table.

3. CALCULATING THE RESONATOR DISPERSION

Soliton solid-state lasers with passive synchronization, including those on a chromium-forsterite crystal, provide stable generation of ultra-short pulses in the

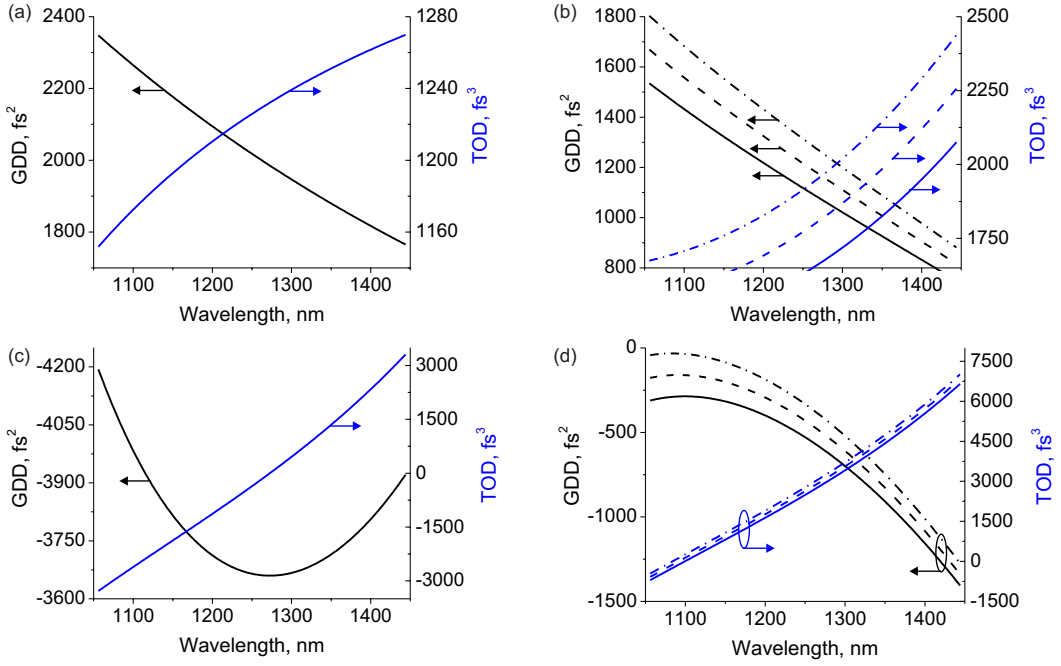

Fig 2. Calculated dependences of GDD (black lines) and TOD (blue lines) of the crystal (*a*), prisms (*b*), prism compressor (*c*), and the entire resonator (*d*). The GDDs and TODs of the individual resonator elements are shown for a single pulse traversal through the resonator. The GDDs (*b*, *d*) are plotted for the prism contribution D_{pr} = 1 100 fs^2 (solid line), 1 200 fs^2 (dashed line), and 1 300 fs^2 (dot-and-dash line) at a wavelength of 1260 nm, corresponding to effective prism thicknesses l_{pr} = of 6.6, 7.2, and 7.8 mm, respectively.

regime of anomalous total GDD of the resonator (Fig. 2), which we will call "solitons" for short.

Formation of such a pulse is due to the effects of nonlinear phase increment mutually compensating for the full bypass of the resonator

$$\phi_{nl} = 2\gamma P l_{cr},$$

where

$$\gamma = \frac{\omega}{c}\frac{n_0 n_2}{A},$$

l_{cr}, n_0, n_2 are the length, linear and nonlinear refractive indices of the crystal, respectively, A is the effective nonlinear mode area in the crystal, and the total dispersive phase overlap

$$\phi_d = \frac{1}{2}\omega_s^2 \sum D_i,$$

where

$$\omega_s^2 = \frac{1}{\tau_s^2} = \left(\frac{1.76}{\tau}\right)^2$$

is the spectral width of the soliton, and τ is the half-height duration, D_i is the group delay dispersion of the i-th element of the resonator. The condition for the existence of the soliton

$$\sum D_i = D_{cr} + D_{pr} + D_{co} < 0, \quad (1)$$

where

$$D_{cr} = \frac{\lambda^3 l_{cr}}{\pi c^3}\frac{\partial^2 n_{cr}}{\partial \lambda^2},$$
$$D_{pr} = \frac{\lambda^3 l_{pr}}{\pi c^3}\frac{\partial^2 n_{pr}}{\partial \lambda^2}, \quad (2)$$
$$D_{co} = -4\frac{\lambda^3 l_{co}}{\pi c^3}\left(\frac{\partial n_{pr}}{\partial \lambda}\right)^2$$

describe the contributions of the material dispersion of the crystal and prisms, as well as the angular dispersion of the prism compressor, respectively [31]. The contribution of the third-order group delay dispersion (TOD), the analysis of which allows us to estimate the supported spectral width of the formed pulses, is calculated by the formula

$$T = \frac{-\lambda^4 l}{2\pi^2 c^3}\left(3\frac{\partial^2 n}{\partial \lambda^2} + \lambda\frac{\partial^3 n}{\partial \lambda^3}\right) \quad (3)$$

for optical elements with thickness l and

$$T_{co} = \frac{-6\lambda^4 l_{co}}{\pi^2 c^3}\frac{\partial n_{pr}}{\partial \lambda}\left(\frac{\partial n_{pr}}{\partial \lambda} + \lambda\frac{\partial^2 n_{pr}}{\partial \lambda^2}\right) \quad (4)$$

for the prism compressor for a complete bypass of the resonator. The material dispersion of SF14 prism glass and forsterite crystal was calculated using the refractive index data in [32, 33]. Taking into account the thicknesses of optical elements and distances between the prisms measured on the bench, the GDD and TOD of the key nodes of the resonator: crystal, prisms, and compressor were plotted (Fig. 2 *a*-*c*). The total GDD was adjusted by moving prism P2 inside the resonator, i.e., by varying the amount of positive dispersion introduced by the material of prism P2. The minimum positive GDD introduced by the material of the two prisms when the pulse double-passed the laser resonator and the beam traveled through the prisms was approximately 1100 fs^2 at a wavelength of 1260 nm (solid black line in Fig. 2 *b*). Fig. 2 *d* shows the calculated group delay dispersion curves for the circular pulse traversal of the entire resonator, corresponding to three P2 prism positions spaced 0.5 mm apart in the direction perpendicular to the beam propagation in the prism, which adds 100 fs^2 per shift. As will be shown later, all stable modes of pulse generation in the laser corresponded to an anomalous GDD of the order from –600 fs^2 to –300 fs^2 in the wavelength region of the crystal gain band, which satisfies the necessary condition for the existence of soliton-like pulses in the resonator.

4. EXPERIMENTAL RESULTS AND THEIR DISCUSSION

As the experience of practical application shows, the highest output average power of the chromophorsterite laser is achieved at the transmission coefficient of the output mirror of about 10% [29, 30, 34, 35], so the studies were started with this mode. Fig. 3 shows spectra 2 and 4 (dashed lines) of the radiation after the output mirror M1 at values of the positive GDD of the prisms at a wavelength of 1260 nm, respectively 1180 fs^2 and 1270 fs^2. Spectra 1, 3, and 5 (solid lines in Fig. 3), recorded after the M5 rotating mirror, at GDD prism values of 720 fs^2, 1180 fs^2, and 1270 fs^2, contain a broad spectral shoulder in the 1400-1500 nm region well outside the gain band of the chromium-sterite laser element.

This feature of the spectrum does not appear after the output mirror M1. When tuning the GDD prisms

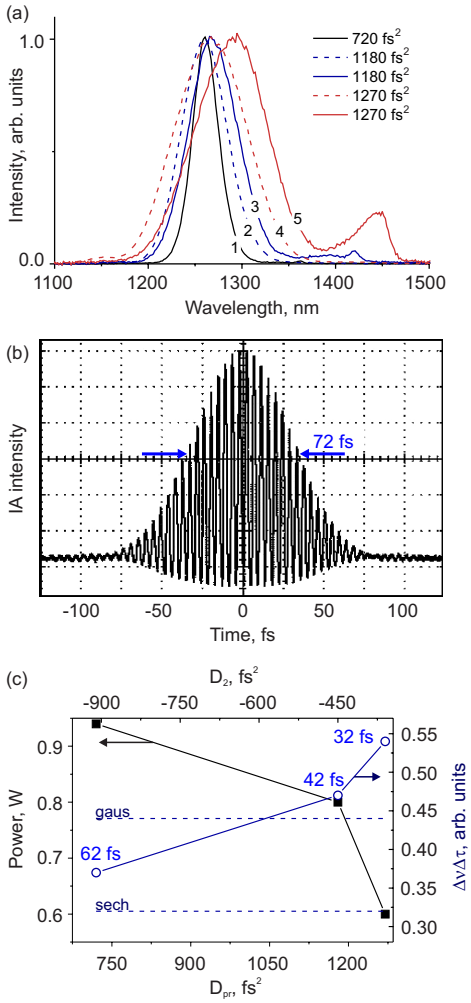

Fig. 3. *a* – Emission spectra of the chrome forsterite laser behind the blanking mirror M1 (dashed lines) and breaking mirror M5 (solid lines) with M1 transmittance of 10% at GDD prisms of 720 fs^2 (black line), 1180 fs^2 (blue lines) and 1260 fs^2 (red lines). *b* – Interference autocorrelation function of pulse intensity (IA) at 1180 fs^2 prism dispersion. *c* – Dependences of average power and product $\Delta\nu\Delta\tau$ of pulses on resonator dispersion.

in a wide range from 720 fs^2 to 1270 fs^2, which corresponded to a shift of 3 mm in the direction perpendicular to the beam, the resonator maintained a stable mode of femtosecond pulse generation without additional alignment of optical elements, changes in pump power and crystal temperature. Fig. 3 *b* shows the autocorrelation function of the pulse after the output mirror M1, which has a duration of about 43 fs, close to the limiting duration (Fig. 3 *b*), at a prism dispersion value of 1180 fs^2. The product of the spectrum width and the duration of the autocorrelation function $\Delta\nu\Delta\tau$ is an important quantity that characterizes the pulse shape. Indeed, for the autocorrelation function shown in Fig. 3 *b*, the product of the spectral width and duration $\Delta\nu\Delta\tau \approx 0.48$, which is close to the value for a spectrally-limited Gaussian-shaped pulse $\Delta\nu\Delta\tau_{gaus} = 0.44$. Reducing the prism contribution to 720 fs^2 leads to the formation of a pulse of about 63 fs duration with more gentle fronts, the shape of which is closer to the shape of the fundamental soliton. This shape is confirmed by the ratio $\Delta\nu\Delta\tau \approx 0.37$, which is close to the ratio for the hyperbolic secant $\Delta\nu\Delta\tau_{sech} = 0.32$ of the fundamental soliton. On the contrary, increasing the contribution of GDD prisms to 1270 fs^2 leads to the formation of radiation with a duration of only about 34 fs with a spectral width of up to 91 nm. Compensation for nonlinear and dispersive phase overlap is very difficult to maintain over such a wide frequency range without residual chirp, which is reflected in the product $\Delta\nu\Delta\tau \approx 0.54$ (Fig. 3 *c*) and distortion of the symmetric pulse shape. Increasing the total GDD of the resonator from –910 fs^2 to –365 fs^2 results in a nearly threefold spectral broadening of the pulse from 32 nm to 91 nm, a decrease in its duration from 63 fs to 34 fs, and in its energy from 9.4 nJ to 6 nJ, giving estimates of the tuning peak radiated power inside the chrome forsterite crystal of 1.5 MW, 1.8 MW, and 1.7 MW. These peak powers come very close to the critical self-focusing power in the forsterite crystal $P_{cr} \approx 7$ MW calculated from $n_2 = 2 \cdot 10^{-16}$ W^{-1}cm^{-2} [36]. Thus, the increase in the intensity of components in the region of 1350-1500 nm in the experiment and the decrease in the average power of the output laser pulses behind the M1 mirror are explained by the arising additional sources of losses in the resonator due to effective nonlinear-optical transformations of radiation. Note that the typical value of energy losses bypassing the resonator due to synchronization of the laser modes by a Kerr lens is about 10^{-5} of the pulse energy [37].

The different position and shape of the spectra after mirrors M1 and M5 at the same value of the resonator dispersion can be caused both by the spectral characteristics of mirrors M1 and M5 and by the different divergence of the spectral components of the main band with the central wavelength of 1260 nm and the Kelly components in the region of 1150 and 1450 nm. The spectra after mirror M1 were recorded in the far zone, and after M5 directly behind the mirror. The measurements of the spectra at different distances from the mirrors M1 and M5 showed that the ratio of the intensities of the bands in the region of 1450 nm and 1250 nm behind the mirror M5 does not depend on the distance from the mirror to the integral sphere of the spectrometer, while the intensity of the band in the region of 1150 nm behind the mirror

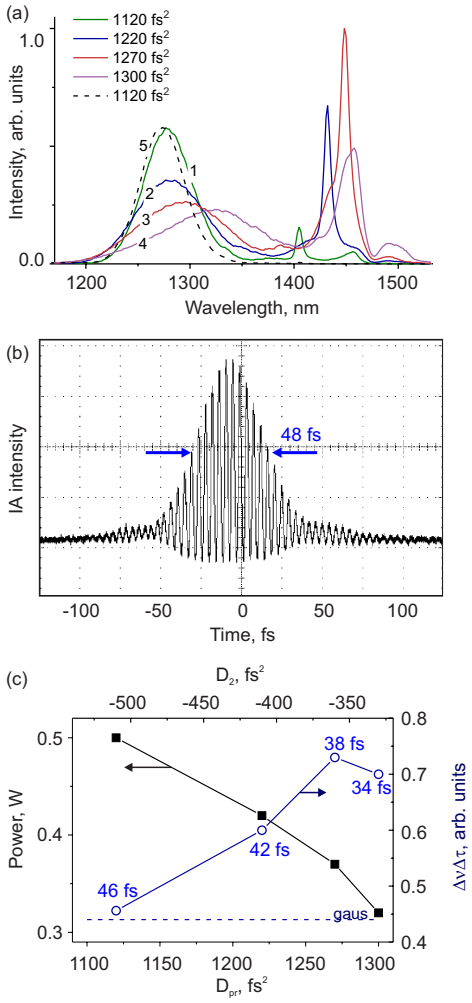

Fig. 4. a – Emission spectra of a chrome forsterite laser behind a blanking mirror M1 (dashed line) and a breaking mirror M5 (solid lines) with M1 transmittance of 5% at GDD prisms of 1120 fs^2 (black and green lines), 1220 fs^2 (blue line), 1270 fs^2 (red line), and 1300 fs^2 (purple line). b – Interference autocorrelation function of pulse intensity (IA) at 1300 fs prism dispersion^2. c – Dependences of average power and ratio $\Delta\nu\Delta\tau$ of pulses on resonator dispersion.

M1 decreases with respect to the intensity of the band in the region of 1250 nm with increasing distance from the mirror. This indicates that the emission in the gain band and the Kelly component in the 1150 nm region have different divergence. The appearance of spectral components in the region of 1150 and 1450 nm is due to the extremely high peak power of radiation in the crystal, leading to the appearance of Kelly peaks in the resonator. Thus, when the GDD of the resonator approaches zero, an additional loss channel of the generated radiation grows in the resonator as a result of energy pumping from the main band to the 1150 and 1450 nm bands. It can also be seen that the maximums in the spectra recorded after mirrors M1 and M5 shift to the long-wavelength region as the prisms's GDD increases, which can be explained by the change in the GDD of the resonator (the total GDD of all elements of the resonator) as the GDD of the prism material increases (Fig. 2).

We then proceeded to analyze the resulting pulses in the laser when the output mirror transmittance was reduced to 5%. The prism dispersion varied from 1120 fs^2 to 1300 fs^2 . Figure 4 shows the pulse spectra in the resonator after the rotating mirror M5 and after the output mirror M1. With the increase of the total GDD of the resonator in the recorded spectra (Fig. 4), there is an increase of components in the 1400-1550 nm band and a decrease of the average laser output power from 500 mW to 320 mW, which corresponds to pulses with energies of 5 and 3.2 nJ. In the correlation functions of the output pulses for all the presented spectra, a positive frequency chirp in the form of "wings" at the edges of the main peak of the correlation function was observed (Fig. 4 *b*) [38]. Increasing the prism dispersion by moving the prisms into the laser beam results in a small duration variation from 47 fs to 35 fs, which corresponds to a variation of the peak pulse power in the resonator from 1.9 to 2.1 MW. The generated pulses have a very large chirp, which is reflected in the variation of the product $\Delta\nu\Delta\tau$ from 0.43 to 0.7 (Fig. 4 *c*) and is explained by the impossibility of perfect phase overlap compensation for pulses with spectral widths up to 80 nm. The interferometric autocorrelation function of such pulses acquires a small "pedestal" (Fig. 4 *b*).

In the case when a highly reflective mirror M1 was installed in place of the output mirror M1, the spectra shown in Fig. 5 were recorded.

Here, putting the prisms into the beam changed the dispersion from 1120 fs^2 to 1320 fs^2. Fig. 5 *b* shows the characteristic autocorrelation function of a pulse with a spectral width of about 90 nm formed at a dispersion of 1280 fs^2. It can be seen that a double-humped pulse structure is formed here, which recognizes the successive strong effects of phase self-modulation and group velocity dispersion, leading to a strong dispersion of the red and blue wings of the spectrum [31]. The passive loss of generated radiation in the forsterite crystal by absorption of radiation at 1250 nm wavelength was about 7%, and the total loss by transmission of radiation at the M1-M5 resonator mirrors was about 1%. It can be seen that the components in the 1400-1550 nm region in the resonator increased significantly, and the energy transfer from the generation band

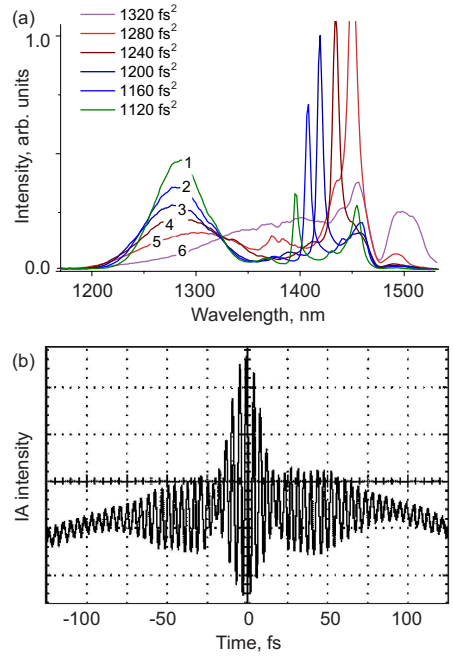

Fig. 5. a – Emission spectra of a chrome forsterite laser behind an M5 breaking mirror (solid lines) with an M1 transmittance of 0.2% at GDD prisms of 1120 fs^2 (green line), 1160 fs^2 (blue line), 1200 fs^2 (blue line), 1240 fs^2 (maroon line), 1280 fs^2 (red line), and 1320 fs^2 (violet line). b – Interference autocorrelation function of the pulse at 1280 fs^2 prism dispersion.

to the Kelly side components increased. In four-wavelength nonlinear optical interaction, as in phase self-modulation of the pulse, new spectral components are formed on both sides of the central wavelength of the pulse. The intensity of the long-wavelength components in the spectrum is much stronger than the short-wavelength components; this is explained by the presence of strong absorption of chrome forsterite in the range up to 1150 nm [39]. For our crystal at the wavelength of 1150 nm, the absorption is 27%. The spectral components in the 1150 nm range, arising from the pumping of pulse energy from the main band at 1250 nm in the process of four-wave interaction and spectral broadening of the generated pulses, also undergo strong absorption in the crystal and do not appear in the spectra behind the M5 mirror against the background of strong bands in the 1250 and 1450 nm region.

To better understand the peculiarities of the pulse energy flow into the lateral components, a theoretical analysis of pulse generation in a laser with passive mode synchronization operating in the quasi-soliton mode of pulse formation was carried out. The excess energy, which arises at the pulse each pass and cannot be encapsulated in the fundamental soliton, can be directed to amplify the dispersive wave located at the frequency ω_{dm} at the periphery of the soliton $\omega_{dm} = \omega_0 \pm \Delta\omega_m$, if its phase ϕ_{dm} differs from the phase of the soliton ϕ_s at $\phi_{dm} - \phi_s = 2\pi m$, where k_j is the dispersion of group velocities j-th order, and the product $k_{2i}l_i$ is the GDD of different sections of the resonator. Soliton phase at the dispersive wavelength

$$\phi_s(\omega_0 \pm \Delta\omega_m) \approx \sum(k_0(\omega_0) \pm k_1\Delta\omega_m - k_2 / (2\tau_s^2))l_i \quad (5)$$

and the phase of the DW itself

$$\phi_{dm}(\omega_0 \pm \Delta\omega_m) \approx$$
$$\approx (k_0(\omega_0) \pm k_{1i}\Delta\omega_m + k_{2i}\Delta\omega_m^2 / 2 \pm k_{3i}\Delta\omega_m^3 / 6))l_i. \quad (6)$$

Using the phase synchronism condition for energy transfer $\phi_{dm} - \phi_s = 2\pi m$, we have

$$3D_2(\Delta\omega_m^2 + \tau_s^{-2}) \pm D_3\Delta\omega_m^3 = 12\pi m, \quad (7)$$

where $D_3 = \sum k_{3i}l_i$. Here we have passed to the total GDD (D_2) and total TOD (D_3) over all elements of the resonator. The case $m = 0$ is not observed in experiments, so we will consider $m = \pm1, \pm2$. When the total third-order dispersion is negligible, $D_3\Delta\omega_m / | D_2 | << 1$, the expression for the nearest position of the Kelly component turns out to be

$$\Delta\omega_1 = \frac{1}{\tau_s}\sqrt{\frac{\pi\tau_s^2}{D_2} - 1}. \quad (8)$$

The minimum Kelly peak frequency detuning observed in experiments from the center of the laser pulse, at which stable pulse generation is still observed, is at least two inverse pulse durations $\Delta\omega_1^{min} \approx 2 / \tau_s$, which gives an estimate for the minimum half-height pulse duration $T_s^{min} \approx 1.1\sqrt{D_2}$. The influence of the peak power of the pulses P on the position of the Kelly side components can be seen if we substitute the condition for the existence of the fundamental soliton

$$\frac{\tau_s^2}{2D_2} = \frac{2l_{cr}}{\gamma P}$$

into equation (8):

$$\Delta\omega_1 = \frac{1}{\tau_s}\sqrt{\frac{4\pi l_{cr}}{\gamma P} - 1}. \quad (9)$$

In the experiment, it is possible to influence the total GDD of the resonator by pushing prisms into the laser beam inside the compressor.

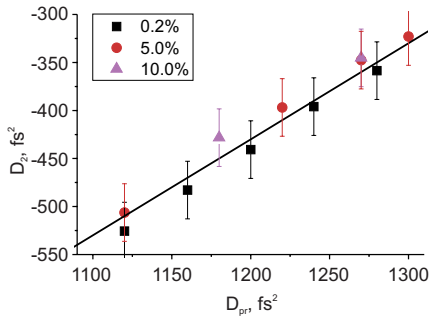

Fig. 6. Calculated (solid line) and experimentally determined by formula (8) through the position of the Kelly spectral components ($\Delta\omega_l$) total GDD of a resonator with an output mirror M1 of 0.2% (black squares), 5% (red circles) and 10% (purple triangles).

In Fig. 6 dots plot the values of the total GDD of the resonator (D_2) calculated by formula (8) from the experimental positions of the Kelly components ($\Delta\omega_l$) shown in Fig. 3-5 at different prism GDDs and output mirror transmittance of 10%, 5%, and 0.2%.

This calculation also required measurement of pulse durations. The accuracy of the dispersion calculation was affected by the large width of the spectrum, which complicates the determination of the central wavelength, the error in determining the pulse durations, and the prism dispersion values. At the same time, for all output mirrors a linear dependence with a uniform slope and slightly different vertical detunings is observed. Also, the calculated total GDD of the resonator, which passes near all experimentally obtained values, was superimposed on this graph. In this way, the connection of the formed narrow spectral lines with the Kelly components was confirmed and the possibility of estimating the total dispersion of the resonator by accurately measuring their position while varying the prism position was shown.

As follows from the experiments, the efficiency of energy pumping from the main band to the 1350-1550 nm range is determined by the total GDD of the resonator and the peak power of pulses in the resonator. The intensity of intracavity pulses is responsible for the efficiency of spectral broadening at soliton dynamics of the pulse in the resonator, and the dispersion of the laser resonator determines the spectral position of the generated pulses and Kelly peaks. Thus, both the growth of the resonator GDD and the growth of the intracavity intensity lead to an increase in the pumping of pulse energy into spectral ranges with low resonator gain. These processes are clearly expressed in the spectra of pulses inside the laser resonator and do not appear in the spectra of pulses after the output mirror due to the spectral characteristics of the mirrors and different divergence of spectral components in the laser gain band and spectral components arising in the resonator as a result of the processes of nonlinear-optical interaction of radiation in the crystal of the active element. Registration of pulse spectra inside the laser resonator allows us to understand which nonlinear-optical processes prevail in the laser and to limit their influence on the generation efficiency when designing the optical scheme of the resonator and pumping parameters. Thus, our work analyzes the measured spectra and durations of radiation at different points of the resonator when varying the transmittance of the laser output mirror. It is shown that at generation of extremely short pulses with duration up to 30 fs with peak power up to 2 MW, spectral broadening of the soliton occurs in the chromium-forsterite crystal, which is the cause of additional passive losses in the laser resonator and limits the obtaining of pulses of the ultimate minimum duration with maximum output power. The presented results are of importance for choosing optimal modes of operation of femtosecond laser oscillators with passive mode synchronization, in particular, on a chrome forsterite crystal.

ACKNOWLEDGEMENTS

The authors express their gratitude to the head of the research group Prof. A. M. Zheltikov for all-round support.

FUNDING

This work was supported by the Russian Science Foundation (grant No. 22-22-00792).

REFERENCES

1. M. D. Perry and G. Mourou, *Science* **264**, 917 (1994).
2. C. N. Danson, C. Haefner, J. Bromage, T. Butcher, J.-C. F. Chanteloup, E. A. Chowdhury, A. Galvanauskas, L. A. Gizzi, J. Hein, and D. I. Hillier, *High Power Laser Science and Engin*. **7**, e54 (2019).
3. R. R. Gattass and E. Mazur, *Nature Photonics* **2**, 219 (2008).
4. T. Steinmetz, T. Wilken, C. Araujo-Hauck, R. Holzwarth, T. W. Hansch, L. Pasquini, A. Manescau, S. D'odorico, M. T. Murphy, and T. Kentischer, *Science* **321**, 1335 (2008).
5. T. Udem, R. Holzwarth, and T. W. Hänsch, *Nature* **416**, 233 (2002).

6. W. R. Zipfel, R. M. Williams, and W. W. Webb, *Nat. Biotech*. **21**, 1369 (2003).
7. S. Yue, M. N. Slipchenko, and J.-X. Cheng, *Laser & Photonics Rev.* **5**, 496 (2011).
8. M.-R. Tsai, S.-Y. Chen, D.-B. Shieh, P.-J. Lou, and C.-K. Sun, *Biomed. Opt. Express* **2**, 2317 (2011).
9. M. Blokker, P. C. de W. Hamer, P. Wesseling, M. L. Groot, and M. Veta, *Sci. Rep.* **12**, 11334 (2022).
10. S. You, H. Tu, E. J. Chaney, Y. Sun, Y. Zhao, A. J. Bower, Y.-Z. Liu, M. Marjanovic, S. Sinha, and Y. Pu, *Nature Commun.* **9**, 2125 (2018).
11. A. A. Lanin, A. S. Chebotarev, I. V. Kelmanson, M. S. Pochechuev, E. S. Fetisova, D. S. Bilan, E. K. Shevchenko, A. A. Ivanov, A. B. Fedotov, and V. V. Belousov, *J. Phys.*: *Photonics* **3**, 044001 (2021).
12. V. Petričević, S. K. Gayen, R. R. Alfano, K. Yamagishi, H. Anzai, and Y. Yamaguchi, *Appl. Phys. Lett.* **52**, 1040 (1988).
13. S.-W. Chu, I.-H. Chen, T.-M. Liu, P. C. Chen, C.-K. Sun, and B.-L. Lin, *Opt. Lett.* **26**, 1909 (2001).
14. C.-K. Sun, S.-W. Chu, S.-Y. Chen, T.-H. Tsai, T.-M. Liu, C.-Y. Lin, and H.-J. Tsai, *J. Struct. Biol.* **147**, 19 (2004).
15. L. V. Doronina-Amitonova, A. A. Lanin, O. I. Ivashkina, M. A. Zots, A. B. Fedotov, K. V. Anokhin, and A. M. Zheltikov, *Appl. Phys. Lett.* **99**, 231109 (2011).
16. M. S. Pochechuev, A. A. Lanin, I. V. Kelmanson, D. S. Bilan, D. A. Kotova, A. S. Chebotarev, V. Tarabykin, A. B. Fedotov, V. V. Belousov, and A. M. Zheltikov, *Opt. Lett.* **44**, 31669 (2019).
17. T. Wang and C. Xu, *Optica* **7**, 947 (2020).
18. A. A. Lanin, A. S. Chebotarev, M. S. Pochechuev, I. V. Kelmanson, D. A. Kotova, D. S. Bilan, Y. G. Ermakova, A. B. Fedotov, A. A. Ivanov, V. V. Belousov, and A. M. Zheltikov, *J. Biophotonics* **13**, e201900243 (2020).
19. A. A. Lanin, M. S. Pochechuev, A. S. Chebotarev, I. V. Kelmanson, D. S. Bilan, D. A. Kotova, V. S. Tarabykin, A. A. Ivanov, A. B. Fedotov, V. V. Belousov, and A. M. Zheltikov, *Opt. Lett.* **45**, 836 (2020).
20. A. A. Lanin, A. S. Chebotarev, M. S. Pochechuev, I. V. Kelmanson, D. A. Kotova, D. S. Bilan, A. A. Ivanov, A. S. Panova, V. S. Tarabykin, A. B. Fedotov, V. V. Belousov, and A. M. Zheltikov, *J. Raman Spectroscopy* **51**, 1942 (2020).
21. P. F. Curley, Ch. Spielmann, T. Brabec, F. Krausz, E. Wintner, and A. J. Schmidt, *Opt. Lett.* **18**, 54 (1993).
22. S. M. J. Kelly, *Electron. Lett.* **28**, 806 (1992).
23. M. L. Dennis and I. N. Duling, *IEEE J. Quantum Electronics* **30**, 1469 (1994).
24. H. A. Haus, *IEEE J. Selected Topics in Quantum Electronics* **6**, 1173 (2000).
25. L. E. Nelson, D. J. Jones, K. Tamura, H. A. Haus, and E. P. Ippen, *App. Phys. B*: *Lasers and Optics* **65**, 277 (1997).
26. M. E. Fermann, M. J. Andrejco, M. L. Stock, Y. Silberberg, and A. M. Weiner, *App. Phys. Lett.* **62**, 910 (1993).
27. K. Tamura, E. P. Ippen, and H. A. Haus, *IEEE Photonics Technology Lett.* **6**, 1433 (1994).
28. J. Li, Y. Wang, H. Luo, Y. Liu, Z. Yan, Z. Sun, and L. Zhang, *Photon. Res. PRJ* **7**, 103 (2019).
29. A. A. Ivanov, A. A. Voronin, A. A. Lanin, D. A. Sidorov-Biryukov, A. B. Fedotov, and A. M. Zheltikov, *Opt. Lett.* **39**, 205 (2014).
30. A. A. Ivanov, G. N. Martynov, A. A. Lanin, A. B. Fedotov, and A. M. Zheltikov, *Opt. Lett.* **45**, 1890 (2020).
31. *Springer Handbook of Lasers and Optics*, ed. By F. Träger, Springer, New York (2012).
32. Z. Burshtein and Y. Shimony, *Opt. Materials* **20**, 87 (2002).
33. Refractive Index of SCHOTT–SF (Dense flint)–SF14, https://refractiveindex.info
34. S.-H. Chia, T.-M. Liu, A. A. Ivanov, A. B. Fedotov, A. M. Zheltikov, M.-R. Tsai, M.-C. Chan, C.-H. Yu, and C.-K. Sun, *Opt. Express* **18**, 24085 (2010).
35. H. Cankaya, S. Akturk, and A. Sennaroglu, *Opt. Lett.* **36**, 1572 (2011).
36. B. Chassagne, A. Ivanov, J. Oberle, G. Jonusauskas, and C. Rulliere, *Opt. Commun.* **141**, 69 (1997).
37. G. Cerullo, S. De Silvestri, and V. Magni, *Opt. Lett.* **19**, 1040 (1994).
38. T. Hirayama and M. Sheik-Bahae, *Opt. Lett.* **27**, 860 (2002).
39. V. Petričević, S. K. Gayen, and R. R. Alfano, *App. Phys. Lett.* **53**, 2590 (1988).